https://doi.org/10.5194/egusphere-2024-1318
Preprint. Discussion started: 23 May 2024

Observing convective activities in the complex organizations and their contributions to the precipitation and anvil amount

Zhenquan Wang[1, *]

[1] School of Atmospheric Sciences, Nanjing University, Nanjing, China

Correspondence to: Zhenquan Wang (zhqwang@smail.nju.edu.cn)

Abstract. The processes of convection precipitating and producing anvil clouds determine the Earth water and radiative budgets. However, convection could have very complicated organizations and behaviors in the tropics. A bunch of convective activities of various life stages would be connected together in the complex organizations and it is difficult to distinguish their behaviors, e.g., precipitating, producing the anvil, merging and splitting. In this work, from the hourly satellite images of the infrared brightness temperature (BT), the organization segments of a single but variable-BT cold core are identified and tracked. By the segment tracking, the detailed evolution of the organization structures (i.e., variations of the cold-core BT, mergers and splits) and the precipitation and anvil contributions of each organization segment are distinguished from the connected convection complex. The results show that the duration, precipitation and anvil amount of the tracked organization segments have a simple log-linear relationship with the cold-core-peak BT. The organization segments of the core colder than 220K are the most robust with the duration of 4-16 hours, while the organization segments of the shallow warmer structures disappear rapidly in a few hours but are the most frequent. The frequency of the mergers and splits also increases exponentially with the decrease of the cold-core-peak BT. By the mergers and splits, more high cloud systems are born from convection and the lifetime-accumulated precipitation and anvil amount are strongly enhanced as compared to those of no mergers and splits. Overall, 85.4% of tropical precipitation are contributed by the long-lived organization segments, in which 67.7% are accompanied with mergers or splits. The tropical non-precipitating anvil amount are mostly contributed by both long-lived organization segments with mergers or splits (49.1%) and fragile warm but frequent organization segments (28.7%).

1. Introduction

Precipitation and anvil clouds are two key components of the convective water budget but usually accompanied with very complicated microphysical and dynamic processes. In climate models, their representation is determined by tunable parameters of large uncertainty, e.g., the detrainment and precipitation efficiency (Rennó et al., 1994; Zhao, 2014; Clement and Soden, 2005; Zhao et al., 2016; Suzuki et al., 2013). In cloud-resolving models, the parameterization scheme is still subject to many uncertainties in ice microphysics and sub-grid turbulence (Matsui et al., 2009; Blossey et al., 2007; Powell et al., 2012; Bretherton, 2015; Atlas et al., 2024), although cloud dynamics and microphysics can be resolved at fine scales. The challenge is partially due to that the detailed processes of convection precipitating and producing anvil clouds have not been sufficiently explored from the observations to advance understanding and model parameterization.

The spatial organization of convection varies from a simple isolated cell to the complex of a bunch of convective activities of various life stages and its variation is closely related to the changes of the precipitation and anvil amount (Yuan and Houze, 2010; Yuan et al., 2011; Tobin et al., 2012; Wing and Emanuel, 2014; Mauritsen and Stevens, 2015; Ruppert and Hohenegger, 2018; Bony et al., 2020; Bao and Sherwood, 2019; Houze, 2004). Cloud-resolving models and observations both suggest that the convective organizations are the important bridge of the interactions between convection and environment (Tobin et al., 2012; Blossey et al., 2005; Coppin and Bony, 2015; Wing and Emanuel, 2014; Wing et al., 2017; Holloway et al., 2017; Muller and Bony, 2015; Sokol and Hartmann, 2022). By the radiative feedback and circulation, the convective organization is associated with the nonconvecting environment. Drier free troposphere and enhanced radiative cooling of the nonconvecting

https://doi.org/10.5194/egusphere-2024-1318
Preprint. Discussion started: 23 May 2024

regions would reinforce the subsidence to expand the dry region and thereby force the convection of the moist region to aggregate (Blossey et al., 2005; Coppin and Bony, 2015). Over the warm oceans, stronger mass convergence and surface turbulent fluxes would promote the aggregation by developing the deep convection and inhibiting scattered convective activities (Coppin and Bony, 2015; Holloway et al., 2017; Wing et al., 2017). The organization variations can influence the precipitation efficiency (Lindzen et al., 2001; Mauritsen and Stevens, 2015; Choi et al., 2017), but under the condition when the total atmospheric water amount is not known, the increased precipitation efficiency does not guarantee the decrease of the anvil amount. Thus, the links between organizations, precipitation and anvils still need further observational evidences as constraints for understanding their climate feedback processes.

Observing the organizations and behaviors of convection is still challenging. Although radar and lidar sensors from polar-orbit satellites or ground-based observatories can penetrate convection, their spatiotemporal sampling is too sparse for tracking. From the images of the brightness temperature at 10.8 μm (BT_{11}) of geostationary satellites (GEOs), pixels of thin cirrus cannot be distinguished from cloudless pixels but the organized convective structures with two distinct modes of deep convection and anvils can be well captured and tracked (Richards and Arkin, 1981; Hendon and Woodberry, 1993; Fu et al., 1990). For the identification of convection, two methods have been proposed in previous studies. One is to identify the contiguous area under a fixed threshold of BT_{11} (Goyens et al., 2011; Schröder et al., 2009; Huang et al., 2018; Williams and Houze, 1987; Chen and Houze, 1997; Kolios and Feidas, 2009; Laing et al., 2008; Feidas and Cartalis, 2007; Fu et al., 2023; Yang et al., 2020; Tsakraklides and Evans, 2003). By the fixed threshold, the complex of connected convection is usually identified to track and it is hard to distinguish convective activities and their contributions to the precipitation and anvils in the complex. Besides, the variable-BT_{11} identification has been proposed in recent years by applying the adaptive BT_{11} thresholds to divide the clustered convection complex into independent convective systems (Yuan and Houze, 2010; Fiolleau and Roca, 2013; Feng et al., 2023; De Laat et al., 2017; Bouniol et al., 2016; Heikenfeld et al., 2019; Zinner et al., 2008; Zinner et al., 2013). This approach brings the possibility to track the detailed variations of the convection organizations but has not been fully achieved, particularly on the aspect of tracking the evolution of the 3-D BT_{11} structures.

Convective systems could merge and split and their BT structures could change rapidly. To determine the life associations between convective systems, one of the most applicable methods is based on the area overlapping rates (Williams and Houze, 1987). This method permits the mergers and splits but has flaws in tracking fast-moving clouds (Huang et al., 2018). Besides, to track the cloud movements, the most widely-used method is based on the cross correlation to match cloud patterns (Leese et al., 1971; Nieman et al., 1997; Velden et al., 1998; Salonen and Bormann, 2016; Hersbach et al., 2020). Those two methods are complementary and usually combined together to first derive cloud displacements and then determine the temporal associations according to the dynamic overlaps (i.e., the overlaps after the movements) (Feng et al., 2023; Zinner et al., 2013).

In this work, the complex convection organizations are segmented and tracked based on the variable-BT_{11} identification and dynamic overlaps. In comparison to the previous tracking algorithms, this work more focuses on the evolution on the BT_{11} dimension. By tracking the organization segments, the aims of this work are twofold: (1) what is the dependence of the duration, precipitation and anvil amount of organization segments on the BT_{11} structures? (2) what are the contributions of organization segments to the tropical precipitation and anvil amount? This paper is laid out as follows: Sect. 2 describes the data and methods used in our analyses; Sect. 3 introduces the variable-BT_{11} segment tracking algorithm and its comparison to the fixed-threshold tracking. Sect. 4 explores the relationship of duration, precipitation and anvil amount of organization segments with the BT_{11} structures and their contributions to the total tropical precipitation and anvil amount.

2. Data and methods

2.1 Images from GEOs

BT_{11} in the tropics between 20°S-20°N and 90°E-190°W was scanned by radiometer imagers on the geostationary Multi-functional Transport Satellite 1 Replacement and 2 Replacement (MTSAT-1R and -2R) with start times at the half an hour and

https://doi.org/10.5194/egusphere-2024-1318
Preprint. Discussion started: 23 May 2024

a view zenith angle less than 60°. The BT_{11} images from 2006 with 1-hour and 8-km resolutions are included in the Satellite ClOud and Radiative Property retrieval System (SatCORPS) of the Clouds and the Earth's Radiant Energy System (CERES) project. In the CERES SatCORPS, BT_{11} was calibrated against the Moderate Resolution Imaging Spectroradiometer (MODIS) from Aqua (Doelling et al., 2013; Doelling et al., 2016). To facilitate the data processing, the BT_{11} images of 8-km pixels were further gridded to 0.05° by linear interpolation (Amidror, 2002).

2.2 Global precipitation measurement (GPM)

At fine scales (0.1° and half-hour resolution), GPM combines all available sensors for precipitation estimates, including microwave imagers from multiple low-Earth orbit satellites, the infrared (IR) channel of GEO radiometers and land-surface rain gauges (Huffman et al., 2007; Huffman et al., 1997). The microwave brightness temperature is sensitive to atmospheric hydrometers for precipitation but has sparse spatiotemporal sampling due to the sun-synchronous orbit. For grid boxes without microwave observations, the GEO-IR BT_{11} is used to estimate precipitation according to the spatially varying calibration coefficient of the microwave precipitation rates (Huffman et al., 1997). To improve the accuracy, rain gauges are further used to rescale the satellite estimates of precipitation rates (Huffman et al., 1997). It has been demonstrated that this satellite-based precipitation product performs well for strong precipitation events with the mean bias smaller than 1 mm/day but misses 20-80% of the light precipitation (< 10 mm/day) (Tian et al., 2009). In the tropics, light precipitation (< 1 mm/hour) accounts for approximately 55-70% of the precipitation area but contributes to only 9-18% of the total precipitation (Yuan and Houze, 2010). Given the large uncertainty in the detection of satellite-based light precipitation but the relatively low importance of total precipitation, only precipitation rates greater than 1 mm/hour are considered as precipitating regions in this work.

2.3 Cloud-top winds from ground-based radar and radiosonde observations

The cloud and wind observations of the radar and radiosondes are combined to derive the cloud-top winds for three tropical ground-based observatories of the Atmospheric Radiation Measurement (ARM) program at Darwin (130.9°E, 12.4°S), Manus Island (147.4°E, 2.1°S) and Nauru Island (166.9°E, 0.5°S). The vertical distribution of hydrometers up to 20 km above the ground is detected by 35 GHz millimeter-wave cloud radar (MMCR) with temporal and spatial sampling of 10 s and 45 m, respectively. The best estimate reflectivity of the MMCR in the range of -50 to 20 dBZ is provided in the ARM program Active Remote Sensing of Clouds (ARSCL) value-added product for the three sites. A reflectivity higher than -40 dBz corresponds to clouds (Zhao et al., 2017). To match the GEO observations, cloud profiles within 5 minutes around the scanning time of the GEO imagers were collected at those three sites, respectively. The 10-min cloud-fraction profile is computed as the ratio of the number of cloud occurrences to the total number of observations at each height. Cloud layers are identified as layers in which the fraction exceeds zero. The thickest cloud layer with the top higher than 5 km and a maximum cloud fraction of at least 50% is selected as the major high cloud layer passing over the sites to collocate with the high clouds observed by GEOs. The cloud top refers to the uppermost height of the cloud layer with the fraction greater than zero.

Winds are detected by the ARM balloon-borne radiosondes with high vertical and temporal resolutions of 10 m and 2.5 s, respectively. The accuracy of the wind speed is approximately 0.5 m/s. The radiosondes are launched two times a day at Manus and Nauru (approximately 11:30 and 23:30 UTC) and four times a day at Darwin (approximately 4:30, 11:15, 16:30 and 23:15 UTC). In comparison with instantaneous cloud detection via the MMCR, balloon-borne radiosondes take hours to drift dozens of kilometers away from the launch location to approach the upper troposphere. To collocate the cloud and wind observations, the difference between the time of cloud-top detection and the time of the balloon-borne radiosondes reaching the cloud top must be within one hour. To match with the tracked motions of the organization segments, the radiosonde cloud-top winds within 150 km of the segment centroids are considered as the observational reference, and the selection of this distance is consistent with previous studies examining the performance of cloud-drift winds (Nieman et al., 1997; Santek et al., 2019; Daniels et al., 2020).

2.4 Comparison of the cloud-top winds and the tracked motions

The difference between the observational cloud-top winds and the tracked motions is assessed by the mean speed and

https://doi.org/10.5194/egusphere-2024-1318
Preprint. Discussion started: 23 May 2024

angle bias, the mean vector difference (MVD), the standard deviation (SD) of the MVD and the root-mean-square error (RMSE), consistent with Nieman et al. (1997):

$$Speed\ BIAS = \frac{1}{N}\sum_{i=1}^{N}\left(\sqrt{U_i^2 + V_r^2} - \sqrt{U_i^2 + V_r^2}\right), \quad (1)$$

$$Angle\ BIAS = \frac{1}{N}\sum_{i=1}^{N}(\arctan\left(\frac{V_i}{U_i}\right) - \arctan\left(\frac{V_r}{U_r}\right)), \quad (2)$$

$$MVD = \frac{1}{N}\sum_{i=1}^{N}\sqrt{(U_i - U_r)^2 + (V_i - V_r)^2}, \quad (3)$$

$$SD = \sqrt{\frac{1}{N}\sum_{i=1}^{N}(\sqrt{(U_i - U_r)^2 + (V_i - V_r)^2} - MVD)^2}, \quad (4)$$

$$RMSE = \sqrt{MVD^2 + SD^2} \quad (5)$$

U and V are the x- and y-component winds, respectively. The subscripts i and r indicate an individual sample of the tracked motion and the corresponding reference winds from the radiosonde observations, respectively, and N is the total number of samples.

2.5 Pattern-matching displacement

The displacement of the organization segment is derived by searching for the maximum similarity of the pattern in the latter image based on cross correlation (Leese et al., 1971; Velden et al., 1998). The target scene is selected as the irregular segment BT_{11} pattern with shapes and is matched in the later image to find the displacement by minimizing the sum of squared differences (SSD) of the normalized BT_{11}:

$$SSD = \sum_{x,y}[BT'_{11}(x,y) - \widetilde{BT}'_{11}(x,y)]^2. \quad (6)$$

$BT'_{11}(x,y)$ and $\widetilde{BT}'_{11}(x,y)$ are the normalized BT_{11} values at pixel (x, y) of the target scene and the cross scene in the search, respectively. By normalizing BT_{11}, the minimum SSD corresponds to the maximum pattern correlation for the BT_{11} structures. The search region is confined by the displacements smaller than 50 km per hour, which is the maximum motion predicted by models (Merrill et al., 1991). The final match is further examined by the coefficient of the pattern correlation. For the areas larger (smaller) than 5000 km^2, the match is valid with a pattern correlation higher than 0.6 (0.8), in which the threshold values are consistent with those of Daniels et al. (2020). Otherwise, the BT_{11} structures would change rapidly and rather be considered to be stationary and the displacement is zero.

2.6 *t* test and confidence intervals

The 95% confidence interval for the mean value was computed based on the t test: $\bar{x} \pm t_c \frac{s}{\sqrt{N}}$. $\bar{x}$ is the mean value of all samples. t_c is the critical value for t. s is the standard deviation of all the samples. N is the number of independent samples, which is determined by the sample length divided by the distance between independent samples (Bretherton et al., 1999).

https://doi.org/10.5194/egusphere-2024-1318
Preprint. Discussion started: 23 May 2024

3. Tracking the convective organization segments

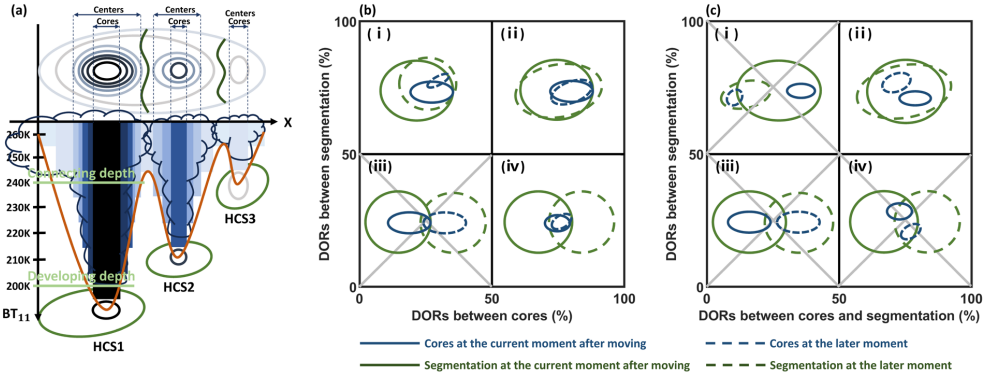

Figure 1. Illustrations of the variable-BT_{11} segment tracking algorithm. (a) Illustrations of segmenting the clustered convection complex into three HCSs as tracking targets, whose 3-D structures in x, y and BT_{11} are captured by the adaptive variable-BT_{11} identification. (b-c) Examples illustrating the temporal associations of HCSs according to the cross overlaps between cores and segmentations. The gray cross indicates the denial of the association.

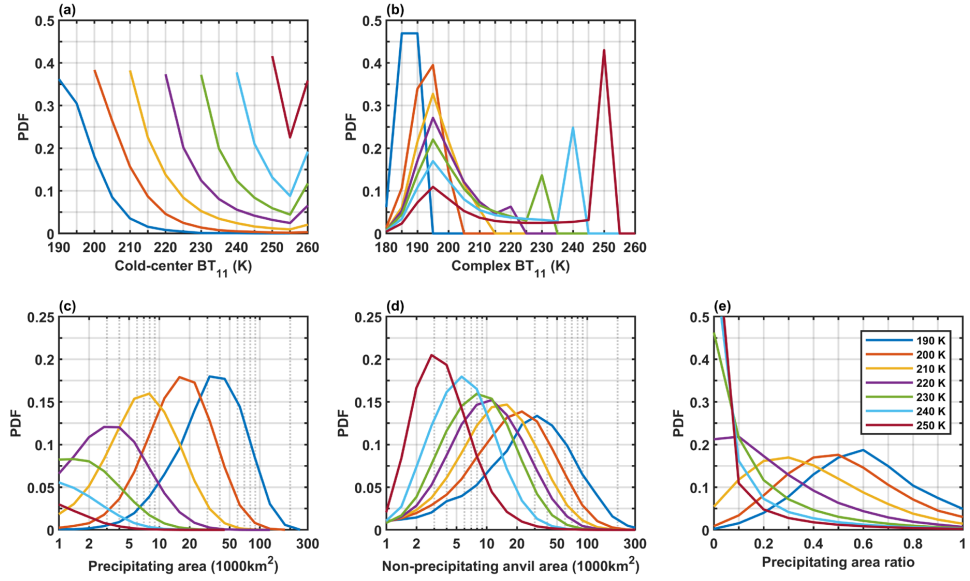

Figure 2. The 3-D structure characteristics of the organization segments. The PDFs of the cold-center BT_{11} (a), complex BT_{11} (b), precipitating area (c), non-precipitating area (d) and precipitating area ratio (e) of the segmented organization structures with the cold-core BT_{11} from 190-250K.

To distinguish the behaviors of the clustered convective activities in the complex organization, the organization segments of high cloud systems (HCSs) with a single but variable-BT_{11} cold core are identified as the tracking targets (Fig. 1a) and further tracked by dynamic overlaps (Fig. 1b-c) from the hourly infrared satellite images. The details of the novel variable-BT_{11} segment tracking algorithm and its difference to the convectional tracking algorithm are described in this section as follows.

As illustrated in Fig. 1a, the connected convection complex could exist in the contiguous area of the BT_{11} colder than 260K. The 260-K BT_{11} threshold would enclose 95% of deep convective clouds and as much of the anvil as possible but has the least contamination from lower-level clouds (Yuan and Houze, 2010; Yuan et al., 2011; Chen and Houze, 1997). A set of adaptive variable-BT_{11} thresholds from 180K to 260K per 5-K interval and the minimum area threshold of 1000km^2 are used

https://doi.org/10.5194/egusphere-2024-1318
Preprint. Discussion started: 23 May 2024

to capture the "growth rings" in the clustered convective complex organizations. As shown in Fig. 1a, these rings reflect the structures in three dimensions of x, y and BT_{11} and are the fundamental indicator of internal dynamics (Houze, 2004). The innermost ring of the local coldest BT_{11} is the cold core of the most active vertically developing region in the HCSs. The isolated ring of the warmest BT_{11} is the cold center and the HCS would be connected (disconnected) to the surrounding HCSs outside (within) the center, and thus the cold-center BT_{11} can indicate the connecting condition of the HCS in the complex organization. Pixels lying outside the centers are assigned to the connected neighborhood HCSs by the 1-K interval to achieve segmentation. The segments have 3-D structures of a single but variable-BT_{11} cold core and its contribution to the precipitation and non-precipitating anvil area can be distinguished from the clustered convective complex organization by the segmentation.

In Fig. 2a, according to the probability distribution functions (PDFs) of the cold-center BT_{11}, it is the most frequent about 35-45% that the cold-center BT_{11} is the same as the cold-core BT_{11} and the isolated deep convective body in the 260-K shield is rare. The isolated structure is less frequent but seems to be another mode for shallow warm systems. Fig. 2b shows the PDFs of the complex BT_{11} that refers to the coldest cold-core BT_{11} in the connected complex. It can be seen that the HCSs of the cold cores of 200-230K are the most frequently clustered in the 195-K complex, and the HCSs of the cores of 220-250K have two modes for the clustered 195-K complex and the isolated shallow warm structures, respectively. This implies the clustered complex organizations are the major mode for the deep convection and thus the segment tracking is necessary to distinguish their behaviors in the complex organizations. By segmentation, Figs. 2c-e show the PDFs of the HCS precipitating and anvil area basically conform to the log-normal distribution and are closely related to the cold-core BT_{11}. The HCSs of colder cores normally contribute to larger precipitating and anvil areas (Fig. 2c-d) but would be more dominated by the precipitation with higher ratios of the precipitating area to the total HCS area (Fig. 2e).

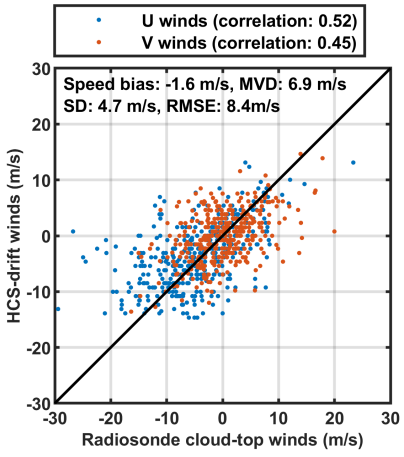

Figure 3. Comparisons of the U and V wind speeds between the tracked motions and radiosonde cloud-top winds within 150km at Darwin, Manus and Nauru in 2006 with a total sample number of 380.

To track the HCS temporal associations, the HCS structure is simply characterized by the core and segmentation and three indices of the core-core, segmentation-segmentation and core-segmentation dynamic overlapping ratios (DORs) are used (Fig. 1b-c). The core and segmentation DORs are relative to the minimum area and represent the degree of the core and segmentation overlaps, respectively. The core-segmentation DORs are relative to the core area and imply whether the core is inherited from the previous HCS. In Fig. 1b, four overlapping situations are distinguished by the core and segmentation DORs exceeding 50% or not. Three situations (i), (ii) and (iv) in Fig. 1b with DORs of either core or segmentation greater than 50% are recognized as the temporal associations, whereas the situation (iii) in Fig. 1b with DORs of both core and segmentation less than 50% disapproves the association of HCSs. In Fig. 1c, when the cores have no overlaps, the association of HCSs relies on the DORs

https://doi.org/10.5194/egusphere-2024-1318
Preprint. Discussion started: 23 May 2024

between segmentation and the DORs of segmentation to cores. In those cases, only situation (ii) in Fig. 1c can be recognized as the HCS association with those two DOR indices both larger than 50%, and the HCSs in the other situations of Fig. 1c are obviously not associated. Thus, the HCS temporal associations are tracked by the conditions of (i), (ii) and (iv) in Fig. 1b and (ii) in Fig. 1c. Mergers and splits are identified by many-to-one and one-to-many associations, respectively.

There are no direct observations for the temporal association. But some of the tracked behaviors (e.g., the tracked motions) can be compared against the observations measured by other sensers. Only if the tracking is correct, would the derived HCS-drift winds perform well. Fig. 3 shows that the HCS-drift winds are significantly correlated with the high-resolution radiosonde winds at the three long-term ARM sites in Darwin, Manus and Nauru within 150 km. The correlation is 0.52 and 0.45 for the U and V wind components, respectively, at the 99% significance level. On average, the HCS-drift winds are slower than the observed ambient winds with the mean bias of -1.6 m/s. The slow speed bias of 1-2 m/s is common in cloud-drift winds (Santek et al., 2019). Due to the limitations of spatial and temporal resolutions (5 km and 1 hour, respectively), the least identifiable speed variation is approximately 5 km/hour (1.4 m/s), which is a possible reason for the slow speed bias. The mean angle bias is very small, approximately 0.5 degrees, and the MVD, SD and RMSE are 6.9, 4.7 and 8.3 m/s, respectively. These biases are not surprising since the real-world clouds do not strictly flow with ambient winds. The RMSE of the vector between the cloud-drift winds and real winds is normally approximately 6-13 m/s according to previous studies (Santek et al., 2019; Bresky et al., 2012). This approves that the tracked motions of the HCSs are reasonable and thus the segment tracking is appropriate.

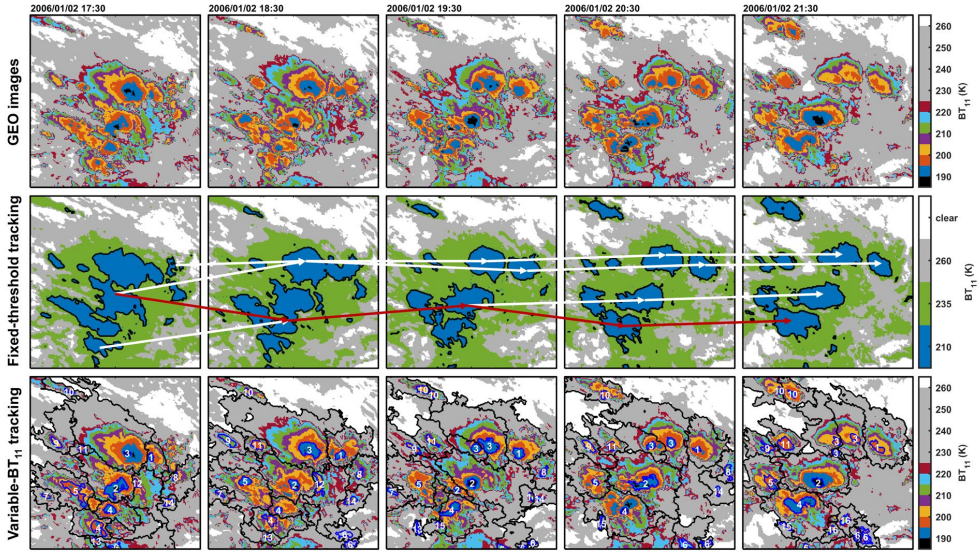

Figure 4. Examples illustrating the difference between the conventional fixed-threshold and the novel variable-BT_{11} segment tracking. Uppermost panel: GEO BT_{11} images taken between 5°S-15°S and 120°E-130°E from January 2 17:30 to 21:30 UTC in 2006. Middle panel: the tracked lifecycles based on the fixed threshold of 210, 235 and 260K. The white lines represent the tree of the tracked temporal associations by the fixed threshold of 210K and the red lines represent the main branch by selecting the largest areas. Bottom panels: the variable-BT_{11} identification and segment tracking. In the bottom panels, the blue contours indicate the cold cores, the black contours are the organization segments in the clustered convection complex, and the number at the core centroids indicates the lifecycle identification.

Examples of the conventional fixed-threshold and novel variable-BT_{11} tracking algorithms are shown in Fig. 4 to illustrate their differences. From the GEO images in the uppermost panel of Fig. 4, it can be visually observed that clustered convections are connected but have distinct behaviors in the complex to decay, split, develop and merge with time. Under the fixed threshold of either 210, 235 or 260K, the convections and their behaviors cannot be distinguished from the complex in the middle panel of Fig. 4. The whole clustered complex organization would be identified as one tracking target by the warm BT_{11} thresholds. By the cold threshold of 210K, only a small cold part of the cluster complex is identified and the connected convections still

https://doi.org/10.5194/egusphere-2024-1318
Preprint. Discussion started: 23 May 2024

cannot be separated but the mergers and splits are caused by whether the convections are connected or disconnected due to the selection of the BT_{11} threshold. In this case, the tree of the tracked temporal associations are too complicated to analyze and usually simplified by only selecting the largest area in each frame as the main branch of the lifecycle. The main branch (the red line in the middle panel of Fig.4) begins with the clustered convection complex that is becoming disconnected with time, and thus ends by less disconnected convection complex. In contrast, with the adaptive variable-BT_{11} identification and segment tracking (the bottom panel of Fig. 4), it is shown that the connected systems are well separated into decaying and splitting No. 3 HCSs, developing No. 2 HCSs, merging and developing No. 4 HCSs, etc. And as illustrated in Fig. 5 the mergers and splits are caused by the evolution of the system structures but not the variations of the connections.

The main difference between the fixed-threshold and variable-BT_{11} segment tracking is the selection of the tracking target. For the fixed-threshold tracking, the tracking target is the 2-D area of the clustered convection complex. For the variable-BT_{11} segment tracking, the tracking target is the 3-D structure of organization segments. The sizes and BT_{11} of the cold core represent the developing strength and the BT_{11} of the cold center represents the connecting conditions, and the segmentation distinguishes the area contribution of the convection in the clustered complex organization.

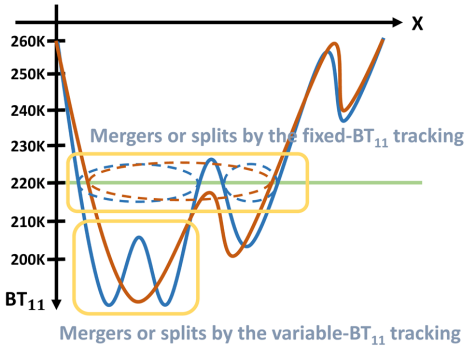

Figure 5. Illustration of the difference for the mergers and splits captured by the variable-BT_{11} tracking and the fixed-threshold tracking. The red and blue lines represent the evolution of the BT_{11} structures of the complex organizations.

4. Contribution of the convective organization segments to the precipitation and anvil amount

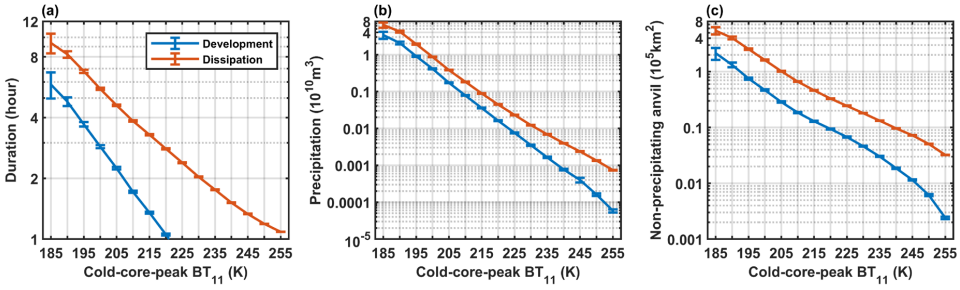

Figure 6. The mean duration (a), precipitation (b) and non-precipitating anvil amount (c) contributed by the organization segments in development (blue lines) and dissipation stages (red lines) with the cold core peaking from 185-255K. respectively. The error bars indicate the 95% confidence intervals of the means based on the t test.

By tracking the organization segments, the detailed convective activities and their contributions to the precipitation and non-precipitating anvil areas can be distinguished from the complex organization. In Fig. 6, the development and dissipation stages of the tracked organization segments are separated by the time of the cold core peaking at the coldest BT_{11} with the largest area. It is interesting that the convective behaviors, i.e., duration, precipitation and producing the non-precipitating anvil clouds, all have a simple log-linear relationship with the peaking BT_{11} in both the development and dissipation stages.

https://doi.org/10.5194/egusphere-2024-1318
Preprint. Discussion started: 23 May 2024

According to the composites of the tracked lifetime (Fig. 6a), in the complex organizations, the segments of the cores colder than 220K would be more robust with the duration of 4-16 hours, while the shallow structures of the warmer cores are fragile and disappear rapidly. Figs. 6b-c also show that the precipitation and anvil clouds in those cold structures are dozens-fold as much as that of the warm structures. It is also noted that more precipitation and anvils are contributed by the dissipation stage of the organization segments and the difference of the duration, precipitation and anvils between two stages has exponential increases with the core peaking at colder BT_{11}. It seems that the convection duration and the two key components of its water budget, precipitation and anvils, are simply determined by its organization structures.

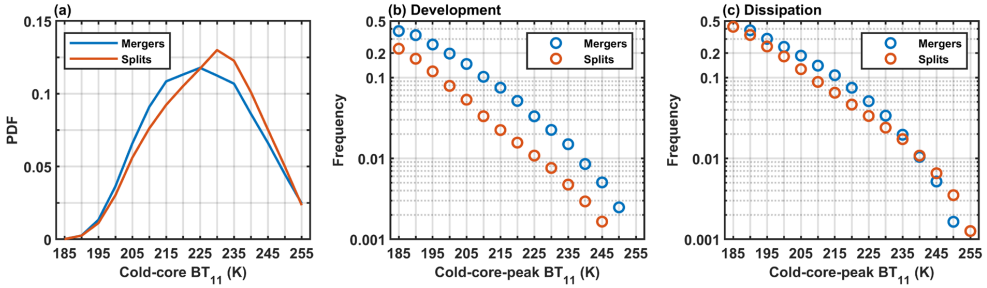

Figure 7. Observed mergers and splits of the convective structures. (a) The PDFs of the merging (the blue line) and splitting (the red line) cold-core BT_{11}. The frequency of the merging and splitting in the evolution of the convection peaking from 185K to 255K in the development (b) and dissipation (c) stages, respectively.

In the conventional fixed-threshold tracking, mergers and splits mostly result from the connection or disconnection of the tracked clustered convective systems. By tracking the segmentation in the clustered complex, the mergers and splits reflect the detailed inner variations of the complex organizations, and represent more HCSs are born from the segmented convection and the complex organizations are clustered by more HCSs, e.g., the No. 4 segment for mergers and the No. 3 segment for splits in the bottom panel of Fig. 4 and the illustration in Fig. 5.

Fig. 7 shows that the mergers and splits are strongly determined by the BT_{11}. On the system level, mergers are relatively more frequent for the cores colder than 225 K and less frequent for the warmer cores as compared with the splits (Fig. 7a). On the lifecycle level, mergers are more frequent than the splits in the development stage (Fig. 7b), and the splits in the dissipation stage (Fig.7c) are more frequent than that in the development stages. In both the development and dissipation stages, it is a bit surprising that the frequency of the mergers and splits still has a log-linear relationship to the cold-core-peak BT_{11}.

How does the mergers and splits influence the precipitation and anvil amount? On the lifecycle level, there would be two possible reasons: the merger and splits influence the precipitation and anvil in the HCSs, or increase the HCS numbers. In Fig. 8, the lifecycles are classified into simple (no mergers and splits), only-merger, only-split and complicated (both mergers and splits) types. Figs. 8a-c show that the total precipitation and non-precipitating anvil area contributed by the tracked convection and its lifetime are strongly related to the occurrence of the mergers and splits. The more complicated the lifecycle is, the larger the precipitation, anvil and lifetime are. Mergers and splits seem to have the same impact on the precipitation and anvil, without significant differences for the lifecycles of only mergers and only splits. Figs. 8d-f decompose the total precipitation and anvil into the contribution from each HCS and the number of the HCSs, respectively, as follows:

$$PN - \bar{P}\bar{N} = \bar{N}P' + \bar{P}N' + P'N', \quad (7)$$

$$AN - \bar{A}\bar{N} = \bar{N}A' + \bar{A}N' + A'N'. \quad (8)$$

P, A and N are the precipitation, non-precipitating anvil areas in each HCS and the HCS numbers, respectively. The bar over the head and prime represent the mean and anomaly, respectively. It is shown that the HCS precipitation is nearly the same no matter whether mergers or splits occur (Fig. 8d) and contributes to -10% (22%) of the variations of the total lifetime precipitation for the peaking core colder (warmer) than 230K (Fig. 8g). In Fig. 8e, some variations of the HCS anvil amount can be found with the occurrence of the mergers and splits but are still relatively small with the mean contribution fraction of

https://doi.org/10.5194/egusphere-2024-1318
Preprint. Discussion started: 23 May 2024

19% to the variation of the total lifetime anvil amount (Fig. 8h). In Fig. 8f-h, on average, the mergers and splits can significantly increase the HCS numbers to contribute to 98% and 67% of the variations of the total lifetime precipitation and anvil amount, respectively. It implies that the mergers and splits could slightly impact the efficiency of precipitating and producing the anvil in each HCS but mainly enhance the lifetime total precipitation and anvil amount by increasing the HCS numbers.

It is also interesting to note that the slope of the log-linear relationship of the precipitation, anvil amount and lifetime to the cold-core-peak BT_{11} is nearly invariant for different types of the lifecycles. It would mean that the mergers and splits do not influence the dependence of the precipitation and anvil on the organization structures and the increased precipitation and anvil by the mergers and splits have to conform to the log-linear relationship to the cold-core-peak BT_{11}.

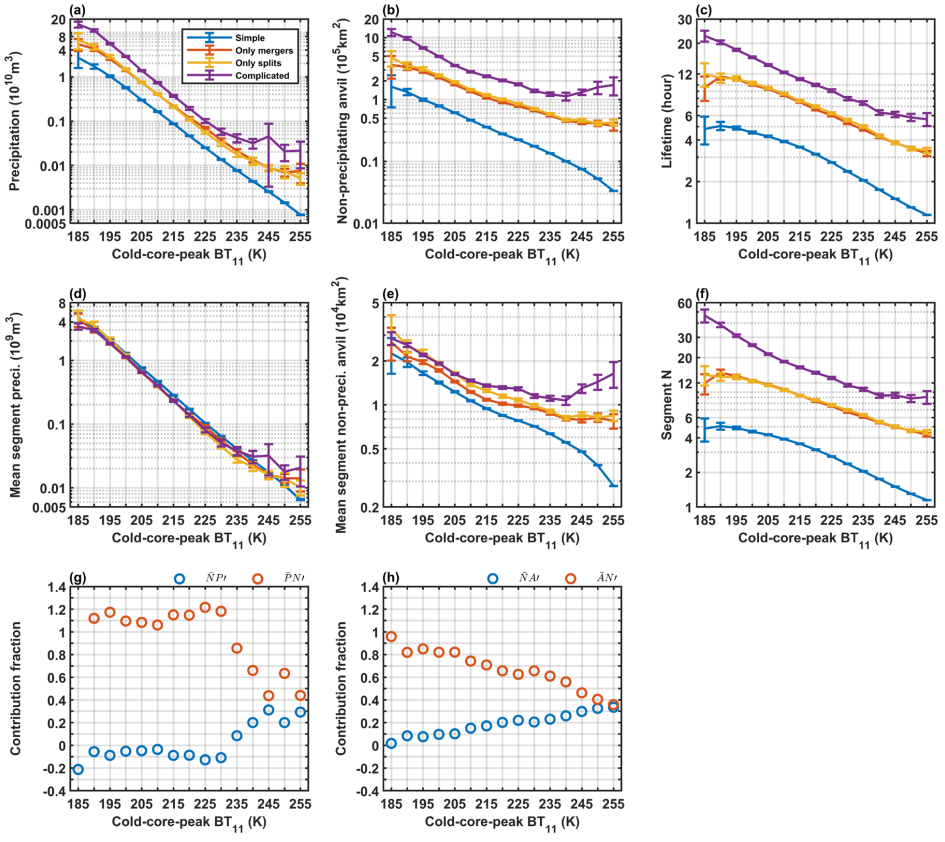

Figure 8. Mean precipitation and anvil amount produced from the whole lifecycle and each single segment, respectively. (a-c) The composites of the precipitation, non-precipitating anvil and lifetime contributed by the whole lifecycles, respectively. (d-e) The composites of precipitation and non-precipitating anvil produced by each segment, respectively. (f) The total number of segments in the tracked lifecycles. (g) The contribution fraction of the segment precipitation and number for the variation of the total lifetime precipitation. (h) The contribution fraction of the segment anvil clouds and number for the variation of the total lifetime anvil amount. The blue, red, yellow and purple lines indicate the simple, only-merger, only-split and complicated lifecycles. The error bars indicate the 95% confidence intervals of the means based on the t test.

https://doi.org/10.5194/egusphere-2024-1318
Preprint. Discussion started: 23 May 2024

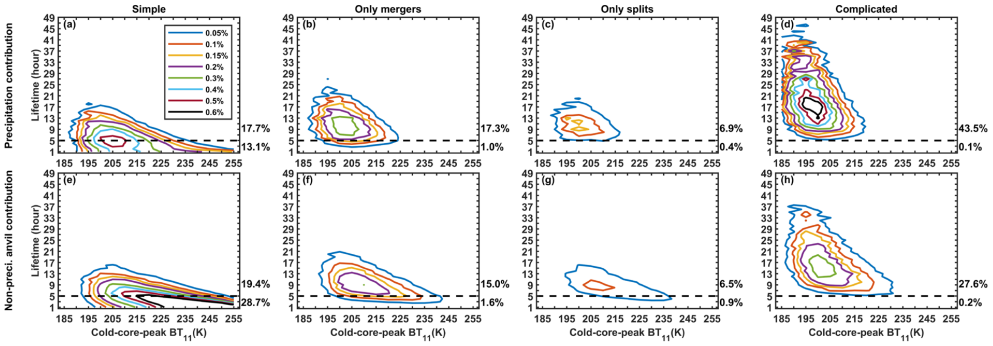

Figure 9. Contribution of the tracked organization segments to the total precipitation and anvil amount. (a-d) Precipitation and (e-h) non-precipitating anvil contribution fraction of the segmented convection of different peaking strength and lifetime, for simple, only-merger, only-split and complicated lifecycles, respectively.

How are the tropical precipitation and anvil associated with the convective organization? Here, the complex organizations have been segmented and tracked. It can be seen from Figs. 6-8 that the precipitation and anvil of the tracked segment would increase exponentially with the colder BT_{11} and are positively related to the occurrence of the mergers and splits, but the warm organization segment (86% of the frequency for the cold-core-peak BT_{11} > 220K) of the lifetime only a few hours are much more frequent than the cold organization segment (14% of the frequency for the cold-core-peak $BT_{11} \leq 220$K). Thus, Fig. 9 distinguishes the contribution of the organization segments to the total precipitation and anvil. In Fig. 9a-d, 94% of precipitation are contributed by the organization segment of the cold-core-peak BT_{11} colder than 220K. 85.4% of precipitation are produced from the long-lived lifecycles (lifetime ≥ 5 hours). The segment of the complicated long-lived lifecycle dominates the largest precipitation fraction of 43.5%, as compared to the simple (30.8%), only-merger (18.3%) and only-split (7.3%) lifecycles. In Fig. 9e-h, the short-lived simple and long-lived complicated organization segments are two most important modes to contribute to 28.7% and 27.6% of the non-precipitating anvil clouds, respectively. On the whole, 68.5% of anvil are produced in the long-lived organization segment, including 19.4% from the simple lifecycles and 49.1% from the lifecycle with mergers and splits. A large portion of anvil (31.4%) is also attributed to the short-lived warm organization segment. Overall, the precipitation is the most associated with the long-lived cold organization segment of complicated lifecycles, while the non-precipitating anvil is the most associated with both the short-lived warm segment (frequent but not efficient to produce anvil) and long-lived cold segments of complicated lifecycles (efficient to produce anvil but not frequent).

5. Conclusion

Tropical convection organizations are normally the connected complex of a bunch of convective activities. In this work, the clustered convection organizations are segmented and further tracked by a novel variable-BT_{11} segment tracking algorithm. The tracked motions of the segments are compared against the observational winds for examining the rationality of the tracking. Strong correlations between the tracked motions and real winds are found with a small difference in the mean speeds (-1.6m/s) and angles (0.5°). These results approve that the tracking is appropriate.

In comparison to the previous tracking algorithms based on the variable-BT_{11} or fixed-BT_{11} identification, instead of only focusing on the 2-D area variations, the 3-D structures of the organization segments (i.e., cold-core and cold-center BT_{11} for indicating the developing and connecting conditions, respectively, and the segmentation for distinguishing the area contribution of each convective activity in the complex) are identified and tracked. In the conventional fixed-threshold tracking, the mergers and splits are easily caused by the connection or disconnection due to the selection of the BT_{11} threshold. But the mergers and splits of the structure body in terms of the same one object are tracked by the novel algorithm and reflect that the more HCSs are born from the convective activity and the cluster number of the complex organizations would increase. Overall, the detailed

https://doi.org/10.5194/egusphere-2024-1318
Preprint. Discussion started: 23 May 2024

variations of the organization structure, especially on the BT_{11} dimension, and the precipitation and anvil contributions of each organization segment can be tracked by the novel algorithm.

It is interesting to note that the duration, precipitation and anvil amount produced from the tracked organization segments have a simple log-linear relationship with the BT_{11} of the cold core peak. The organization segments of the cold core less than 220K are the most robust with the duration 4-16 hours, while the warmer organization segments are fragile to disappear rapidly but with the occurrence frequency as high as 86% in the complex. On the lifecycle level, more precipitation and anvil amount are contributed in the decaying stage of the organization segments as compared to that in the development stage. The difference between two stages would increase exponentially with the decrease of the cold-core-peak BT_{11}. The occurrence of the mergers and splits also strongly depend on the BT_{11} of the cold core peak with a log-linear relationship. Overall, the mergers are more frequent at the colder cores in the development stages as compared to the splits, and the splits are more frequent in the decaying stages than that in the development stage. The organization segments accompanied with the mergers and splits would produce more precipitation and anvil as compared to that with no mergers and splits. By the mergers and splits, more HCSs are born from the convection but on the lifecycle average the precipitation and anvil in each HCS only have small variations. The results show that for the complicated lifecycles 98% and 67% of the precipitation and anvil increases, respectively, are attributed to the increase of the HCS numbers. It is also interesting to note that the slope of the log-linear relationship between the lifetime precipitation or anvil and the cold-core-peak BT_{11} is almost invariant in simple and complicated lifecycles.

For the total water budget in the complex convection organizations, the organization segments of cold structures and long-lived lifecycles with mergers or splits contribute to the largest fraction of the precipitation and non-precipitating anvil amount, 67.7% and 49.1%, respectively. The warm short-lived organization segments contribute to little precipitation but relatively a high fraction of non-precipitating anvil (28.7%) due to its high frequency.

Acknowledgment

This work was supported by the NSFC-41875004 and the National Key R&D Program of China (2016YFC0202000).

Author contribution

ZW designed the algorithm and prepared the manuscript.

Data and code availability

All data used in this study are available online. The GEO images (Nasa/Larc/Sd/Asdc, 2017) are obtained from the National Aeronautics and Space Administration (NASA) Langley Research Center Atmospheric Science Data Center (https://search.earthdata.nasa.gov/). GPM (Huffman, 2023) is obtained from the Goddard Earth Sciences Data and Information Services Center (GES DISC). The ground-based cloud (S. Giangrande, 1999) and wind (E. Keeler, 2001) observations at the ground-based sites are obtained from the Atmospheric Radiation Measurement user facility, a U.S. Department Of Energy (DOE) office of science user facility managed by the biological and environmental research program (https://www.arm.gov). The code of the anvil tracking algorithm is available upon request.

Competing interests

The author declares no conflict of interest.

Reference

Amidror, I.: Scattered data interpolation methods for electronic imaging systems: a survey, Journal of Electronic Imaging, 11, 10.1117/1.1455013, 2002.

Atlas, R. L., Bretherton, C. S., Sokol, A. B., Blossey, P. N., and Khairoutdinov, M. F.: Tropical Cirrus Are Highly Sensitive to Ice Microphysics Within a Nudged Global Storm-Resolving Model, Geophysical Research Letters, 51, 10.1029/2023gl105868, 2024.

https://doi.org/10.5194/egusphere-2024-1318
Preprint. Discussion started: 23 May 2024

Bao, J. and Sherwood, S. C.: The Role of Convective Self-Aggregation in Extreme Instantaneous Versus Daily Precipitation, Journal of Advances in Modeling Earth Systems, 11, 19-33, 10.1029/2018ms001503, 2019.

Blossey, P. N., Bretherton, C. S., and Khairoutdinov, M.: An Energy-Balance Analysis of Deep Convective Self-Aggregation above Uniform SST, Journal of the Atmospheric Sciences, 62, 4273-4292, 10.1175/jas3614.1, 2005.

Blossey, P. N., Bretherton, C. S., Cetrone, J., and Kharoutdinov, M.: Cloud-Resolving Model Simulations of KWAJEX: Model Sensitivities and Comparisons with Satellite and Radar Observations, Journal of the Atmospheric Sciences, 64, 1488-1508, 10.1175/jas3982.1, 2007.

Bony, S., Semie, A., Kramer, R. J., Soden, B., Tompkins, A. M., and Emanuel, K. A.: Observed Modulation of the Tropical Radiation Budget by Deep Convective Organization and Lower-Tropospheric Stability, AGU Advances, 1, 10.1029/2019av000155, 2020.

Bouniol, D., Roca, R., Fiolleau, T., and Poan, D. E.: Macrophysical, Microphysical, and Radiative Properties of Tropical Mesoscale Convective Systems over Their Life Cycle, Journal of Climate, 29, 3353-3371, 10.1175/jcli-d-15-0551.1, 2016.

Bresky, W. C., Daniels, J. M., Bailey, A. A., and Wanzong, S. T.: New Methods toward Minimizing the Slow Speed Bias Associated with Atmospheric Motion Vectors, Journal of Applied Meteorology and Climatology, 51, 2137-2151, 10.1175/jamc-d-11-0234.1, 2012.

Bretherton, C. S.: Insights into low-latitude cloud feedbacks from high-resolution models, Philos Trans A Math Phys Eng Sci, 373, 10.1098/rsta.2014.0415, 2015.

Bretherton, C. S., Widmann, M., Dymnikov, V. P., Wallace, J. M., and Bladé, I.: The Effective Number of Spatial Degrees of Freedom of a Time-Varying Field, Journal of Climate, 12, 1990-2009, 10.1175/1520-0442(1999)012<1990:Tenosd>2.0.Co;2, 1999.

Chen, S. S. and Houze, R. A.: Diurnal variation and life-cycle of deep convective systems over the tropical pacific warm pool, Quarterly Journal of the Royal Meteorological Society, 123, 357-388, 10.1002/qj.49712353806, 1997.

Choi, Y. S., Kim, W., Yeh, S. W., Masunaga, H., Kwon, M. J., Jo, H. S., and Huang, L.: Revisiting the iris effect of tropical cirrus clouds with TRMM and A-Train satellite data, Journal of Geophysical Research: Atmospheres, 122, 5917-5931, 10.1002/2016jd025827, 2017.

Clement, A. C. and Soden, B.: The Sensitivity of the Tropical-Mean Radiation Budget, Journal of Climate, 18, 3189-3203, 10.1175/jcli3456.1, 2005.

Coppin, D. and Bony, S.: Physical mechanisms controlling the initiation of convective self-aggregation in a General Circulation Model, Journal of Advances in Modeling Earth Systems, 7, 2060-2078, 10.1002/2015ms000571, 2015.

Daniels, J., Bresky, W., Bailey, A., Allegrino, A., Velden, C. S., and Wanzong, S.: Chapter 8 - Winds from ABI on the GOES-R Series, in: The GOES-R Series, edited by: Goodman, S. J., Schmit, T. J., Daniels, J., and Redmon, R. J., Elsevier, 79-94, https://doi.org/10.1016/B978-0-12-814327-8.00008-1, 2020.

de Laat, A., Defer, E., Delanoë, J., Dezitter, F., Gounou, A., Grandin, A., Guignard, A., Meirink, J. F., Moisselin, J.-M., and Parol, F.: Analysis of geostationary satellite-derived cloud parameters associated with environments with high ice water content, Atmospheric Measurement Techniques, 10, 1359-1371, 10.5194/amt-10-1359-2017, 2017.

Doelling, D. R., Sun, M., Nguyen, L. T., Nordeen, M. L., Haney, C. O., Keyes, D. F., and Mlynczak, P. E.: Advances in Geostationary-Derived Longwave Fluxes for the CERES Synoptic (SYN1deg) Product, Journal of Atmospheric and Oceanic Technology, 33, 503-521, 10.1175/jtech-d-15-0147.1, 2016.

Doelling, D. R., Loeb, N. G., Keyes, D. F., Nordeen, M. L., Morstad, D., Nguyen, C., Wielicki, B. A., Young, D. F., and Sun, M.: Geostationary Enhanced Temporal Interpolation for CERES Flux Products, Journal of Atmospheric and Oceanic Technology, 30, 1072-1090, 10.1175/jtech-d-12-00136.1, 2013.

E. Keeler, K. B. a. J. K.: Balloon-Borne Sounding System (SONDEWNPN), ARM Data Center, 10.5439/1595321, 2001.

Feidas, H. and Cartalis, C.: Application of an automated cloud-tracking algorithm on satellite imagery for tracking and monitoring small mesoscale convective cloud systems, International Journal of Remote Sensing, 26, 1677-1698, 10.1080/01431160512331338023, 2007.

https://doi.org/10.5194/egusphere-2024-1318
Preprint. Discussion started: 23 May 2024

Feng, Z., Hardin, J., Barnes, H. C., Li, J., Leung, L. R., Varble, A., and Zhang, Z.: PyFLEXTRKR: a flexible feature tracking Python software for convective cloud analysis, Geoscientific Model Development, 16, 2753-2776, 10.5194/gmd-16-2753-2023, 2023.

Fiolleau, T. and Roca, R.: An Algorithm for the Detection and Tracking of Tropical Mesoscale Convective Systems Using Infrared Images From Geostationary Satellite, IEEE Transactions on Geoscience and Remote Sensing, 51, 4302-4315, 10.1109/tgrs.2012.2227762, 2013.

Fu, R., Del Genio, A. D., and Rossow, W. B.: Behavior of Deep Convective Clouds in the Tropical Pacific Deduced from ISCCP Radiances, Journal of Climate, 3, 1129-1152, 10.1175/1520-0442(1990)003<1129:Bodcci>2.0.Co;2, 1990.

Fu, Y., Sun, J., Fu, S., Zhang, Y., and Ma, Z.: Initiations of Mesoscale Convective Systems in the Middle Reaches of the Yangtze River Basin Based on FY-4A Satellite Data: Statistical Characteristics and Environmental Conditions, Journal of Geophysical Research: Atmospheres, 128, 10.1029/2023jd038630, 2023.

Goyens, C., Lauwaet, D., Schröder, M., Demuzere, M., and Van Lipzig, N. P. M.: Tracking mesoscale convective systems in the Sahel: relation between cloud parameters and precipitation, International Journal of Climatology, 32, 1921-1934, 10.1002/joc.2407, 2011.

Heikenfeld, M., Marinescu, P. J., Christensen, M., Watson-Parris, D., Senf, F., van den Heever, S. C., and Stier, P.: tobac 1.2: towards a flexible framework for tracking and analysis of clouds in diverse datasets, Geoscientific Model Development, 12, 4551-4570, 10.5194/gmd-12-4551-2019, 2019.

Hendon, H. H. and Woodberry, K.: The diurnal cycle of tropical convection, Journal of Geophysical Research, 98, 10.1029/93jd00525, 1993.

Hersbach, H., Bell, B., Berrisford, P., Hirahara, S., Horányi, A., Muñoz-Sabater, J., Nicolas, J., Peubey, C., Radu, R., Schepers, D., Simmons, A., Soci, C., Abdalla, S., Abellan, X., Balsamo, G., Bechtold, P., Biavati, G., Bidlot, J., Bonavita, M., Chiara, G., Dahlgren, P., Dee, D., Diamantakis, M., Dragani, R., Flemming, J., Forbes, R., Fuentes, M., Geer, A., Haimberger, L., Healy, S., Hogan, R. J., Hólm, E., Janisková, M., Keeley, S., Laloyaux, P., Lopez, P., Lupu, C., Radnoti, G., Rosnay, P., Rozum, I., Vamborg, F., Villaume, S., and Thépaut, J. N.: The ERA5 global reanalysis, Quarterly Journal of the Royal Meteorological Society, 146, 1999-2049, 10.1002/qj.3803, 2020.

Holloway, C. E., Wing, A. A., Bony, S., Muller, C., Masunaga, H., L'Ecuyer, T. S., Turner, D. D., and Zuidema, P.: Observing Convective Aggregation, Surveys in Geophysics, 38, 1199-1236, 10.1007/s10712-017-9419-1, 2017.

Houze, R. A.: Mesoscale convective systems, Reviews of Geophysics, 42, 10.1029/2004rg000150, 2004.

Huang, X., Hu, C., Huang, X., Chu, Y., Tseng, Y.-h., Zhang, G. J., and Lin, Y.: A long-term tropical mesoscale convective systems dataset based on a novel objective automatic tracking algorithm, Climate Dynamics, 51, 3145-3159, 10.1007/s00382-018-4071-0, 2018.

Huffman, G. J., Adler, R. F., Bolvin, D. T., Gu, G., Nelkin, E. J., Bowman, K. P., Hong, Y., Stocker, E. F., and Wolff, D. B.: The TRMM Multisatellite Precipitation Analysis (TMPA): Quasi-Global, Multiyear, Combined-Sensor Precipitation Estimates at Fine Scales, Journal of Hydrometeorology, 8, 38-55, 10.1175/jhm560.1, 2007.

Huffman, G. J., Adler, R. F., Arkin, P., Chang, A., Ferraro, R., Gruber, A., Janowiak, J., McNab, A., Rudolf, B., and Schneider, U.: The Global Precipitation Climatology Project (GPCP) Combined Precipitation Dataset, Bulletin of the American Meteorological Society, 78, 5-20, 10.1175/1520-0477(1997)078<0005:Tgpcpg>2.0.Co;2, 1997.

Huffman, G. J., E.F. Stocker, D.T. Bolvin, E.J. Nelkin, Jackson Tan: GPM IMERG Final Precipitation L3 Half Hourly 0.1 degree x 0.1 degree V07, Goddard Earth Sciences Data and Information Services Center (GES DISC), 10.5067/GPM/IMERG/3B-HH/07, 2023.

Kolios, S. and Feidas, H.: A warm season climatology of mesoscale convective systems in the Mediterranean basin using satellite data, Theoretical and Applied Climatology, 102, 29-42, 10.1007/s00704-009-0241-7, 2009.

Laing, A. G., Carbone, R., Levizzani, V., and Tuttle, J.: The propagation and diurnal cycles of deep convection in northern tropical Africa, Quarterly Journal of the Royal Meteorological Society, 134, 93-109, 10.1002/qj.194, 2008.

Leese, J. A., Novak, C. S., and Clark, B. B.: An Automated Technique for Obtaining Cloud Motion from Geosynchronous Satellite Data Using Cross Correlation, Journal of Applied Meteorology, 10, 118-132, 10.1175/1520-

https://doi.org/10.5194/egusphere-2024-1318
Preprint. Discussion started: 23 May 2024

0450(1971)010<0118:Aatfoc>2.0.Co;2, 1971.

Lindzen, R. S., Chou, M.-D., and Hou, A. Y.: Does the Earth Have an Adaptive Infrared Iris?, Bulletin of the American Meteorological Society, 82, 417-432, 10.1175/1520-0477(2001)082<0417:Dtehaa>2.3.Co;2, 2001.

Matsui, T., Zeng, X., Tao, W.-K., Masunaga, H., Olson, W. S., and Lang, S.: Evaluation of Long-Term Cloud-Resolving Model Simulations Using Satellite Radiance Observations and Multifrequency Satellite Simulators, Journal of Atmospheric and Oceanic Technology, 26, 1261-1274, 10.1175/2008jtecha1168.1, 2009.

Mauritsen, T. and Stevens, B.: Missing iris effect as a possible cause of muted hydrological change and high climate sensitivity in models, Nature Geoscience, 8, 346-351, 10.1038/ngeo2414, 2015.

Merrill, R. T., Menzel, W. P., Baker, W., Lynch, J., and Legg, E.: A Report on the Recent Demonstration of NOAA's Upgraded Capability to Derive Cloud Motion Satellite Winds, Bulletin of the American Meteorological Society, 72, 372-376, 10.1175/1520-0477-72.3.372, 1991.

Muller, C. and Bony, S.: What favors convective aggregation and why?, Geophysical Research Letters, 42, 5626-5634, 10.1002/2015gl064260, 2015.

NASA/LARC/SD/ASDC: SatCORPS CERES GEO Edition 4 MTSAT-1R Version 1.0, NASA Langley Atmospheric Science Data Center DAAC, 2017.

Nieman, S. J., Menzel, W. P., Hayden, C. M., Gray, D., Wanzong, S. T., Velden, C. S., and Daniels, J.: Fully Automated Cloud-Drift Winds in NESDIS Operations, Bulletin of the American Meteorological Society, 78, 1121-1133, 10.1175/1520-0477(1997)078<1121:Facdwi>2.0.Co;2, 1997.

Powell, S. W., Houze, R. A., Kumar, A., and McFarlane, S. A.: Comparison of Simulated and Observed Continental Tropical Anvil Clouds and Their Radiative Heating Profiles, Journal of the Atmospheric Sciences, 69, 2662-2681, 10.1175/jas-d-11-0251.1, 2012.

Rennó, N. O., Emanuel, K. A., and Stone, P. H.: Radiative-convective model with an explicit hydrologic cycle: 1. Formulation and sensitivity to model parameters, Journal of Geophysical Research: Atmospheres, 99, 14429-14441, 10.1029/94jd00020, 1994.

Richards, F. and Arkin, P.: On the Relationship between Satellite-Observed Cloud Cover and Precipitation, Monthly Weather Review, 109, 1081-1093, 10.1175/1520-0493(1981)109<1081:Otrbso>2.0.Co;2, 1981.

Ruppert, J. H. and Hohenegger, C.: Diurnal Circulation Adjustment and Organized Deep Convection, Journal of Climate, 31, 4899-4916, 10.1175/jcli-d-17-0693.1, 2018.

S. Giangrande, E. C. a. P. K.: Active Remote Sensing of CLouds (ARSCL1CLOTH), ARM Data Center, 10.5439/1996113, 1999.

Salonen, K. and Bormann, N.: Atmospheric Motion Vector observations in the ECMWF system: Fifth year report, 2016.

Santek, D., Dworak, R., Nebuda, S., Wanzong, S., Borde, R., Genkova, I., García-Pereda, J., Galante Negri, R., Carranza, M., Nonaka, K., Shimoji, K., Oh, S. M., Lee, B.-I., Chung, S.-R., Daniels, J., and Bresky, W.: 2018 Atmospheric Motion Vector (AMV) Intercomparison Study, Remote Sensing, 11, 10.3390/rs11192240, 2019.

Schröder, M., König, M., and Schmetz, J.: Deep convection observed by the Spinning Enhanced Visible and Infrared Imager on board Meteosat 8: Spatial distribution and temporal evolution over Africa in summer and winter 2006, Journal of Geophysical Research: Atmospheres, 114, 10.1029/2008jd010653, 2009.

Sokol, A. B. and Hartmann, D. L.: Congestus Mode Invigoration by Convective Aggregation in Simulations of Radiative-Convective Equilibrium, J Adv Model Earth Syst, 14, e2022MS003045, 10.1029/2022MS003045, 2022.

Suzuki, K., Golaz, J. C., and Stephens, G. L.: Evaluating cloud tuning in a climate model with satellite observations, Geophysical Research Letters, 40, 4464-4468, 10.1002/grl.50874, 2013.

Tian, Y., Peters-Lidard, C. D., Eylander, J. B., Joyce, R. J., Huffman, G. J., Adler, R. F., Hsu, K. l., Turk, F. J., Garcia, M., and Zeng, J.: Component analysis of errors in satellite-based precipitation estimates, Journal of Geophysical Research: Atmospheres, 114, 10.1029/2009jd011949, 2009.

Tobin, I., Roca, R., and Bony, S.: Observational Evidence for Relationships between the Degree of Aggregation of Deep Convection, Water Vapor, Surface Fluxes, and Radiation, Journal of Climate, 25, 6885-6904, 10.1175/jcli-d-11-00258.1, 2012.

https://doi.org/10.5194/egusphere-2024-1318
Preprint. Discussion started: 23 May 2024

Tsakraklides, G. and Evans, J. L.: Global and regional diurnal variations of organized convection, Journal of Climate, 16, 1562-1572, Doi 10.1175/1520-0442-16.10.1562, 2003.

Velden, C. S., Olander, T. L., and Wanzong, S.: The Impact of MultispectralGOES-8Wind Information on Atlantic Tropical Cyclone Track Forecasts in 1995. Part I: Dataset Methodology, Description, and Case Analysis, Monthly Weather Review, 126, 1202-1218, 10.1175/1520-0493(1998)126<1202:Tiomgw>2.0.Co;2, 1998.

Williams, M. and Houze, R. A.: Satellite-Observed Characteristics of Winter Monsoon Cloud Clusters, Monthly Weather Review, 115, 505-519, 10.1175/1520-0493(1987)115<0505:Socowm>2.0.Co;2, 1987.

Wing, A. A. and Emanuel, K. A.: Physical mechanisms controlling self-aggregation of convection in idealized numerical modeling simulations, Journal of Advances in Modeling Earth Systems, 6, 59-74, 10.1002/2013ms000269, 2014.

Wing, A. A., Emanuel, K., Holloway, C. E., and Muller, C.: Convective Self-Aggregation in Numerical Simulations: A Review, Surveys in Geophysics, 38, 1173-1197, 10.1007/s10712-017-9408-4, 2017.

Yang, R., Zhang, Y., Sun, J., and Li, J.: The comparison of statistical features and synoptic circulations between the eastward-propagating and quasi-stationary MCSs during the warm season around the second-step terrain along the middle reaches of the Yangtze River, Science China Earth Sciences, 63, 1209-1222, 10.1007/s11430-018-9385-3, 2020.

Yuan, J. and Houze, R. A.: Global Variability of Mesoscale Convective System Anvil Structure from A-Train Satellite Data, Journal of Climate, 23, 5864-5888, 10.1175/2010jcli3671.1, 2010.

Yuan, J., Houze, R. A., and Heymsfield, A. J.: Vertical Structures of Anvil Clouds of Tropical Mesoscale Convective Systems Observed by CloudSat, Journal of the Atmospheric Sciences, 68, 1653-1674, 10.1175/2011jas3687.1, 2011.

Zhao, M.: An Investigation of the Connections among Convection, Clouds, and Climate Sensitivity in a Global Climate Model, Journal of Climate, 27, 1845-1862, 10.1175/jcli-d-13-00145.1, 2014.

Zhao, M., Golaz, J. C., Held, I. M., Ramaswamy, V., Lin, S. J., Ming, Y., Ginoux, P., Wyman, B., Donner, L. J., Paynter, D., and Guo, H.: Uncertainty in Model Climate Sensitivity Traced to Representations of Cumulus Precipitation Microphysics, Journal of Climate, 29, 543-560, 10.1175/jcli-d-15-0191.1, 2016.

Zhao, W., Marchand, R., and Fu, Q.: The diurnal cycle of clouds and precipitation at the ARM SGP site: Cloud radar observations and simulations from the multiscale modeling framework, Journal of Geophysical Research: Atmospheres, 122, 7519-7536, 10.1002/2016jd026353, 2017.

Zinner, T., Mannstein, H., and Tafferner, A.: Cb-TRAM: Tracking and monitoring severe convection from onset over rapid development to mature phase using multi-channel Meteosat-8 SEVIRI data, Meteorology and Atmospheric Physics, 101, 191-210, 10.1007/s00703-008-0290-y, 2008.

Zinner, T., Forster, C., de Coning, E., and Betz, H. D.: Validation of the Meteosat storm detection and nowcasting system Cb-TRAM with lightning network data – Europe and South Africa, Atmospheric Measurement Techniques, 6, 1567-1583, 10.5194/amt-6-1567-2013, 2013.